NUCLEAR ENGINEERING AND TECHNOLOGY
ISSN / eISSN 1738-5733
Publisher KOREAN NUCLEAR SOC, NUTOPIA BLDG,
342-1 JANGDAE-DONG, DAEJEON, SOUTH KOREA,
Volume 26-Issue 1-(2026)
DOI:https://doi.org/10.65613/736835

OPEN ACCESS

Development and Characterization of a Zirconia-Reinforced Calcium Phosphate-Based Biocomposite

Check for updates

Saida Bouyegh [1]*, Latifa Kahloul [2], Soundes Kelaiaia [2]

[1]Research Center in Industrial Technologies (CRTI), P.O. Box 64, Cheraga, Algiers 16014, Algeria

[2] National Higher School of Technology and Engineering, Laboratory of Mining, Metallurgy and Materials (L3M), Annaba 23005, Algeria

*** Corresponding Author Email:** sbouyegh@yahoo.fr

Received : 23/02/2026 ; Accepted : 26/05/2026

Abstract

Due to its improved bioactivity and biocompatibility, hydroxyapatite (HA) is a biomaterial that is frequently used for implant applications. However, hydroxyapatite ceramics can only reach their full potential if their comparatively poor mechanical qualities are strengthened, especially through the creation of composite materials. In this study, HA–zirconia composites were prepared and evaluated with the aim of developing calcium phosphate (CaP) composites reinforced with stabilized zirconia. Based on its exceptional mechanical qualities and biocompatibility, zirconia (ZrO_2) particles were chosen as the reinforcing phase.Natural bovine bone was used to extract hydroxyapatite, which offers a sustainable and eco-friendly source of phosphocalcic bioceramic material. To create dense ceramic bodies, composites with varying ZrO_2 percentages were agglomerated and then sintered for three hours at 1150 °C. The prepared composites were characterized using scanning electron microscopy (SEM), energy-dispersive spectroscopy (EDS), differential scanning calorimetry (DSC), X-ray diffraction (XRD), Fourier-transform infrared spectroscopy (FTIR), and instrumented hardness testing. XRD analysis showed that HA decomposed into calcium oxide (CaO) and β-tricalcium phosphate (β-TCP). During sintering, these decomposition products are combined with ZrO_2 to create calcium zirconate ($CaZrO_3$). Additionally, a non-uniform distribution of the yttria-stabilized zirconia (YSZ) phase within the HA matrix was shown by microstructural investigations, which affected the mechanical properties of the HA/YSZ composites.

Keywords : Hydroxyapatite, Zirconia, Bovine bone, Composite, Sintering.

1. Introduction

Calcium phosphates (CaP) are the main mineral constituent of human bones and teeth. Given their very high chemical similarity to the inorganic component of natural bone, their biocompatibility, non-toxicity and tunable biodegradability, calcium phosphate bioceramics appear as ideal candidates in the biomedical field [1, 2]. Calcium phosphate-based ceramics in a wide variety of forms and compositions are currently in use or being considered in many areas of dentistry and orthopedics, and others are still under development [3-6].

However, the fragile nature of these bioceramics does not allow them to be used in load-bearing areas, such as artificial teeth or bones [7-11]. To overcome this drawback and to improve the reliability of these bioceramics, biocomposites and hybrid biomaterials have been manufactured using various reinforcements (ceramic, metallic or polymer) [12]. Many researchers have used several methods and various (bioinert) materials for strengthening calcium phosphates, such as alumina [13], titanium [14] and silica [15] nanoparticles, to increase mechanical efficiency.

The incorporation of bioinert materials into calcium phosphate increases properties such as hardness, toughness and fracture toughness of composites [16, 17]. Among the many reinforcements, zirconium oxide (ZrO_2) is one of the best known materials due to its high biocompatibility, chemical resistance, hardness and fracture toughness [18, 19]. Several reinforcement approaches, using a bioactive matrix of biocompatible calcium phosphate, and a bioinert zirconia material, have been explored to improve bone regeneration and mechanical stability. According to recent work, Cao et al. [20] prepared a mixture of HA and 3YSZ obtained by a flash sintering process to avoid phase degradation and promote densification for mechanical stability. It is in this context that we opted for the economical and environmentally friendly "green" approach to synthesize calcium phosphate bioceramic (CaP) by valorizing biowaste such as bovine bones and adding bioactive zirconia at a low percentage by weight to refine the microstructure of HA and reduce the crystallization temperature of HA.

2. Experimental details

2.1 Material

2.1.1 Preparation of Phosphocalcium (HA) Bioceramic:

In this study, the phosphocalcium raw material was extracted from biowaste, namely bovine femur bones, using a thermal decomposition process. The bovine femur bones (Figure 1) were collected from a local butcher shop. The hydroxyapatite produced from bovine bones was compared to synthetic hydroxyapatite from Sigma-Aldrich (289396, Sigma-Aldrich, USA).

Figure 1. Raw bovine femur bones.

The preparation of the CaP powder (HA) was carried out following the method of Barakat et al. [21] with some modifications. First, the spongy bones (the extremities) were discarded, and the bone fragments were soaked in water for 24 hours to drain the blood. The surface flesh of the bones was then cut away with a scalpel. Next, using a household blowtorch and applying a direct flame to the cleaned bone, the organic components were burned off. The bones were then boiled in water using a household pressure cooker. This procedure was repeated several times with fresh water. The bones were washed and rinsed several times with water to ensure the complete removal of attached meat, tendons, bone marrow, and other soft tissues. They were then immersed in acetone for 2 hours and subsequently washed with distilled water to remove any remaining invisible fats. Finally, the bones were dried in a vacuum oven at 60°C for 3 days to evaporate the absorbed moisture. A calcination process was carried out in a two-temperature air muffle furnace (Nabertherm) at 400 and 900 °C. The process was performed in an atmospheric muffle furnace for 3 hours, with the temperature ramps set at 5 °C/min. Heating to 400 °C was performed to ensure the complete elimination of organic compounds and to prevent microbial contamination. Following this process, the bones turned black because they still contained charcoal due to the combustion of organic components. The bone powder was then calcined at 900 °C to ensure the complete combustion of organic matter and to lower its specific surface area. This process transformed the black ash into a white powder.

The zirconia was recovered from a dental zirconia disc at a dentist's office to be used as reinforcement.

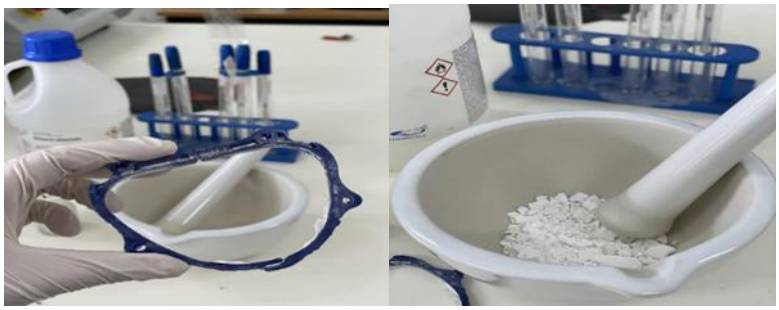

Figure 2. Dental zirconia disc

2.1.2 HA/YSZ composites preparation

To achieve this, two raw materials were used: calcium phosphate, specifically hydroxyapatite, as the matrix, and zirconia (ZrO_2) as reinforcement. The procedure followed is as follows:

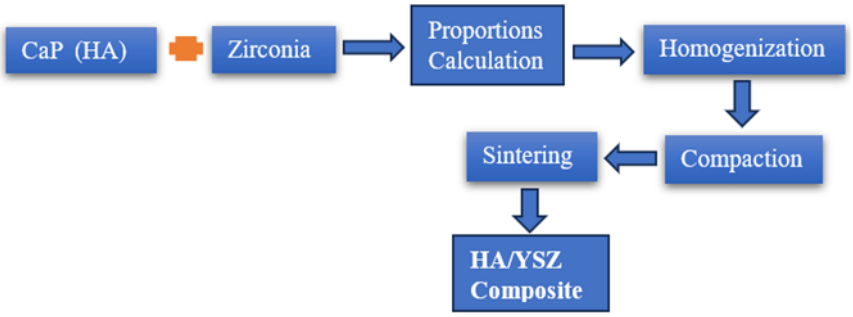

Figure 3. Methodology for Composite Development.

Formulation of the composites' constituent proportions

Following the calcination of the powders (bone, zircone, and synthetic HA) at 900 °C for two hours, each powder was weighed. First, the percentages of zirconia and HA for each composite were calculated. The ZrO_2 (YSZ) and HA powders were then weighed in accordance with the mass ratios specified in the following table:

Tableau 1. The weight of each component

Sample code	HA (% W)	ZrO_2 (% W)	HA (g)	ZrO_2 (g)
HA	100	-	3g	-
HA + 5% ZrO_2	95	5	2,85	0,15
HA + 10% ZrO_2	90	10	2,7g	0,3
HA + 20% ZrO_2	80	20	2,4g	0,6
HA + 30% ZrO_2	70	30	2,1g	0,9
ZrO_2	-	100	-	3

2.2 Characterization methods

A variety of characterization techniques have been established, including infrared spectroscopy, X-ray diffraction, SEM-EDS analysis, and calorimetry essential to balayage (DSC/ATG), which are complementary analyses for studying the physical-chemical properties of materials and advanced composites. Phase formation for the deposited coatings was investigated by XRD on a Bruker D8 diffractometer using Cu Kα radiation (λ = 1.5418 Å) in a (θ–2θ) Bragg Brentano geometry, range from of 10°–90° with a step size of 0.01. Transform Infrared (FT-IR) spectra were performed in the mid-infrared range 4000–400 cm^{-1} at room temperature using Shimadzu-8400 FT-IR spectroscopy from the Chemistry Department laboratory at Badji Mokhtar University of Annaba. The number of scans was 16 and the resolution was 4 cm^{-1}. The hardness and Young's modulus of the sintered samples were evaluated by instrumented hardness tests, carried out by applying a load of 3N using a macrohardness tester (ZWICK ZHU2.5) at the Foundry Laboratory (LRF), Badji Mokhtar University Annaba. The morphology and microstructure of the sintered samples were observed with a scanning electron microscope of type Quanta 250-FEI of the ENSM-Annaba, coupled with an EDAX detector allowing the performance of EDS microanalysis.

3. Results and discussion

3.1 Structural Characteristics

Figure 4 shows the SEM morphology of hydroxyapatite powder produced from bovine bone, synthetic HA, and zirconia. It is clear that the bovine powder has an almost spherical morphology. In contrast, the zirconia powder exhibits an irregular morphology with varying particle sizes, indicating a wide range of particle sizes, which could be related to the manufacturing method. Furthermore, the synthetic HA powder has a rounded morphology and very fine particles.

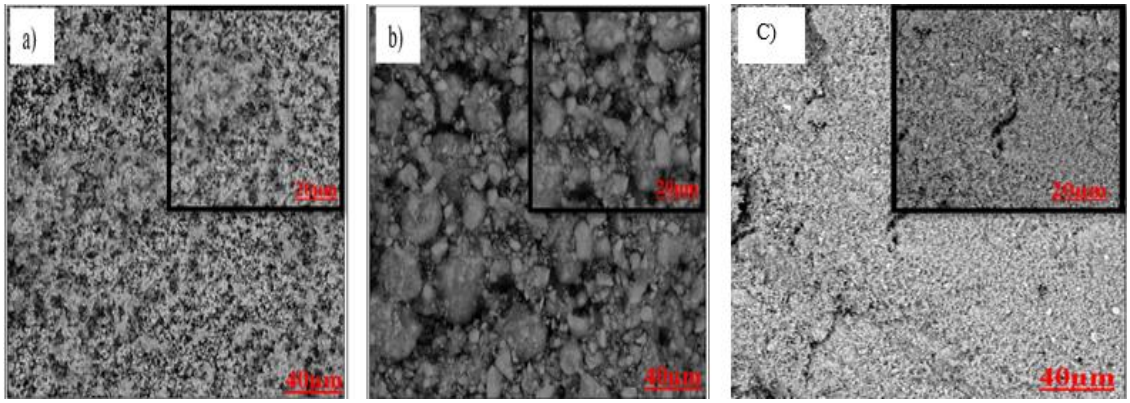

Figure 4. SEM morphology of the hydroxyapatite powder: a) elaborated (bovine) b) synthetic HA c) Zirconia

3.2 EDS Analysis

EDS analysis allows us to obtain the average composition of the prepared powders (bovine) and the powders used (zirconia and synthetic HA); the result of this analysis is given in Figure 5.

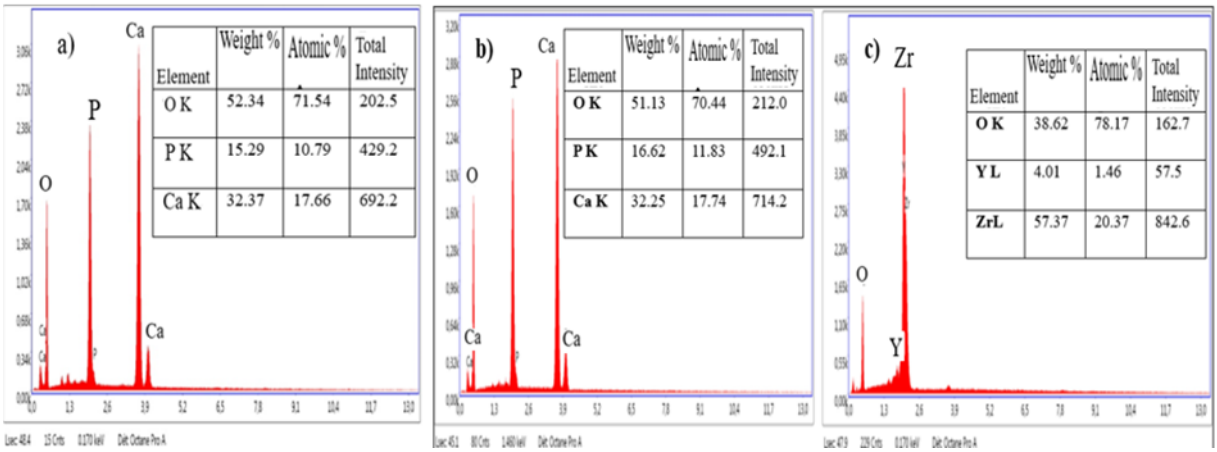

Figure 5. EDS analysis (a) Bovine hydroxyapatite: BHA, (b) Synthetic hydroxyapatite: SHA, (c) Zirconia

The result of this analysis confirms the presence of the components of hydroxyapatite, namely calcium, phosphorus and oxygen, with a percentage greater than 50% for O_2 and a percentage less than 50% for Ca and

P. also it confirms the components of synthetic HAp (Ca, P, O) and that the Ca/P ratio differs from the characteristic value of 1.67 for stoichiometric HA. Regarding the zirconia components (Zr, Y, O), the presence of Y indicates that the zirconia used is yttrium-stabilized.

3.2. Structural characteristics of fritted composites:

Numerous factors affect the sintired physical characteristics, including the powder's characteristics (morphology, dimensions, purity, etc.), the thermal treatment circumstances (temperature, duration, pressure, etc.), and the treatment atmosphere (vide, different protective atmospheres, etc.).

The microstructures of pastilles frittered at 1150 °C for 03 hours are shown in Figure 6. Three stages are taken into consideration throughout the sintering process: the final stage is the rearrangement of the grains, which brings them closer to one another and creates bridges. This stage is completed for relative densities over 65%. The first step involves eliminating open porosity and, thus, increasing pore diameters. She spreads until it reaches a relative density of 92–95%. Above this relative density of transition, the stage occurs. It involves the elimination of closed porosity and coalescence.

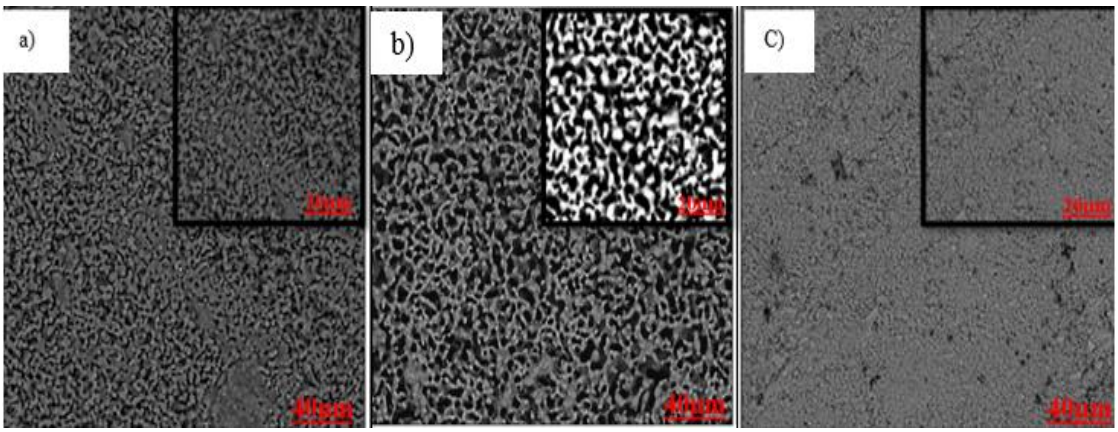

Figure 6. SEM morphology of sintered a) HA. HA de bovin, b) HA synthesis, and c) zirconia

The SEM analysis shown in Figure 6 reveals an evolution in porosity forms and phases compared to non-fritted powder. The micrographs demonstrate grain boundary formation and the presence of porosity due to incomplete densification of the ceramics at this temperature. Additionally, the observations show a heterogeneous dispersion of grains. It is also noteworthy that the morphology of the three HA from different sources is similar. Zirconia morphology, as seen by scanning electron microscopy consists of spherical agglomerates of grains of varying sizes.

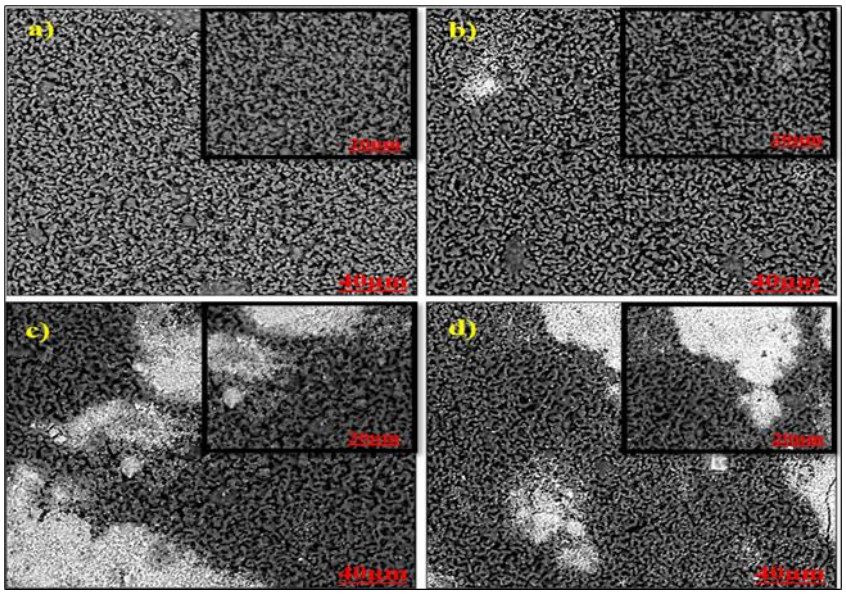

Figure 7. SEM morphology of sintered composites. a) HA+ 5% ZrO_2, b) HA+10% ZrO_2, c) HA+ 20% ZrO_2, d) HA+ 30% ZrO_2.

Figure 7 shows a variety of micrographs. SEM of developed composite surfaces at 1150 °C. It is possible to see a change in porosity and phase, which can be attributed to the interaction between hydroxyapatite and zirconia. The crucial factor in their densification is evident. The dark areas represent the hydroxyapatite phase, while the clear areas are associated with zirconia. This illustrates the creation of a composite HA-zirconia using traces of zirconia as reinforcing material and a HA component acting as a matrix. Porous microstructures have been found in a variety of samples. It is possible to say that the observed micrographies have a porous appearance with interspersed granules.

3.2.2 Analyse EDS :

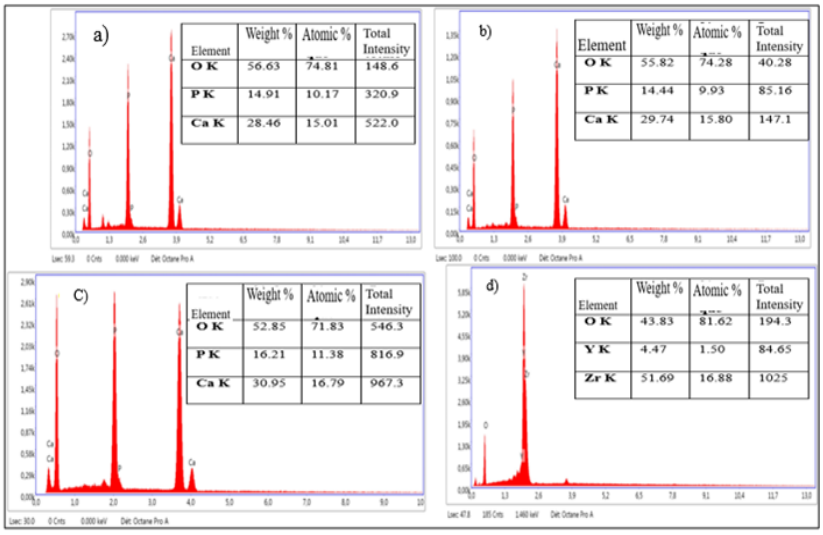

Figure 8. EDS analysis of sintered composites a) HA+ 5% ZrO_2. b) HA+ 10% ZrO_2, C) HA+ 20% ZrO_2, d) HA+ 30% ZrO_2.

The chemical composition of phosphocalcic composites reinforced with zirconium by MDP is analyzed using EDS in parallel to the acquisition in SEM. The obtained EDX spectra are shown in Figure 8. The percentage of ZrO_2 and Y in each composite has increased. The composite HA 5% ZrO_2 has the lowest percentage of stabilized zirconia, with values of 12% ZrO_2 and 0.38% Y, while the composite HA 30% ZrO_2 has the highest percentage of stabilized zirconia, with values of 28,53% ZrO_2 and 1.46% Y_3**.**

3.3 Phase identification by X-ray diffraction (XRD):

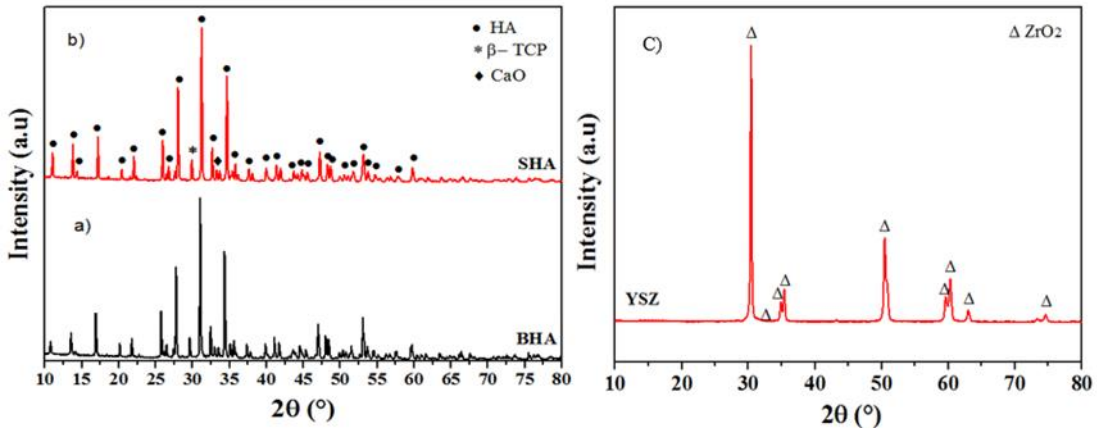

Figure 9. Spectres XRD (a) Bovine hydroxyapatite: BHA, (b) Synthetic hydroxyapatite: SHA, (c) Zirconia

The X-ray diffraction lines are fine and reflect the good crystallization of the prepared products calcined at 1150 °C. This shows that the high-temperature heat treatment results in well-crystallized apatites. According to the ICDD records, the X-ray diffraction analysis (Figure 9) indicates that the material extracted from the bone corresponds to hydroxyapatite, unlike synthetic (commercial) hydroxyapatite. The characteristic peaks of HA were compared to the JCPDS standard files. A hexagonal hydroxyapatite (HA) with a primitive lattice is associated with JCPDS file No. 09-0432 [22, 23]. Figure 9(c) indicates that 3YSZ appears as a major phase. An orthorhombic zirconia structure with a primitive lattice correlated to JCPDS file no. 87-2105 was obtained.

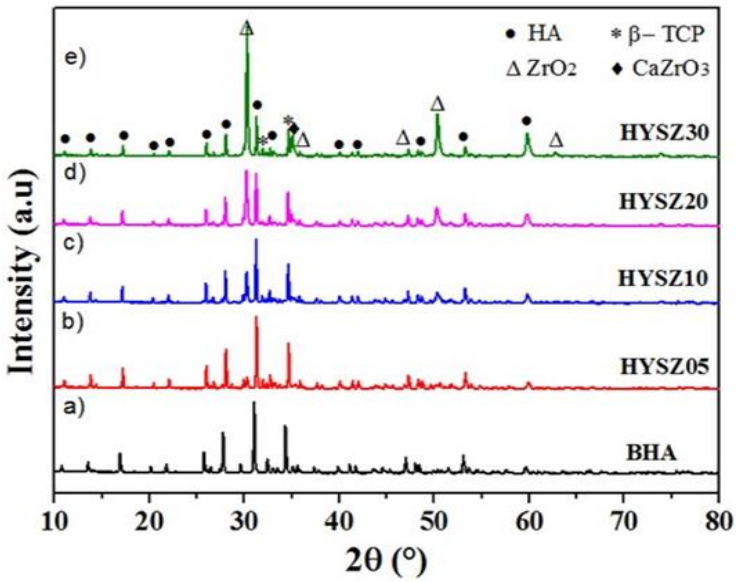

Figure 10. XRD spectra of HA-based composites sintered 1150°C/ 3h. (a) : BHA, (b) : BHA+ 5 % YSZ, (c) :BHA+ 10 % YSZ, (d) : BHA+ 20 % YSZ, (e) : BHA+ 30 % YSZ.

The X-ray diffraction (XRD) spectra of HA-zirconia-based composites sintered at 1150 °C/3 h are shown in Figures 10. For HA-based composites containing ZrO_2, the XRD spectra show distinct peaks for HA and zirconia, indicating the formation of HA-zirconia composites. The XRD spectra revealed that the major phase in all samples is HA. However, the beta-tricalcium phosphate (β-TCP) phase was observed as a minor phase. This minor phase is often detected in high-temperature sintered HA ceramics [24]. Indeed, HA was decomposed into (β-TCP) and CaO, which reacts with ZrO_2 to form calcium zirconate ($CaZrO_3$). HA was decomposed into β-TCP, CaO, and water vapor. With the release of excess CaO through further decomposition of HA, the solubility of Ca in ZrO_2 exceeds the maximum solid solution range, and $CaZrO_3$ is formed [25, 26]. This HA decomposition in the presence of ZrO_2 can be explained by the following equation:

$$CaO + ZrO_2 \rightarrow CaZrO_3$$

Indeed, increasing zirconia concentration showed a trend toward increased intensity (Figure 10), while the reduction in maximum HA intensity could be attributed to an alteration in HA texture with respect to ZrO_2 concentration [27]. These results are in good agreement with those reported by [25, 26, 28] for HA-ZrO_2 composites.

3.4 Fourier Transform Infrared Spectroscopy (FTIR):

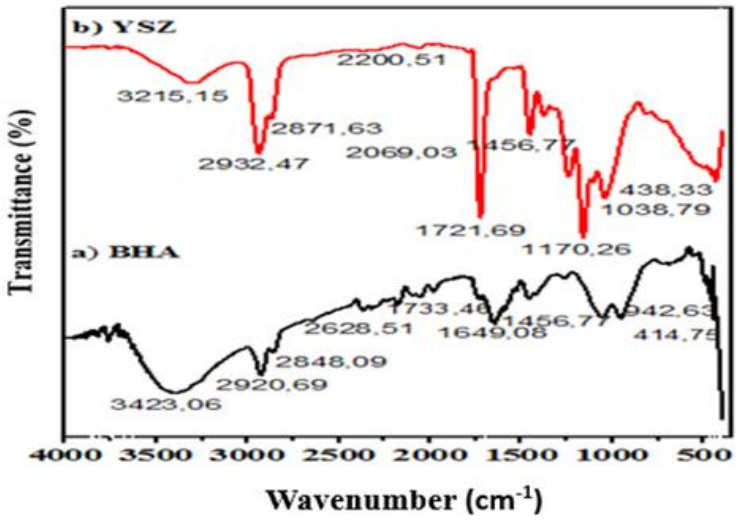

Figure 11. Fourier Transform Infrared (FTIR) Spectroscopy (a) BHA ; (b) YSZ

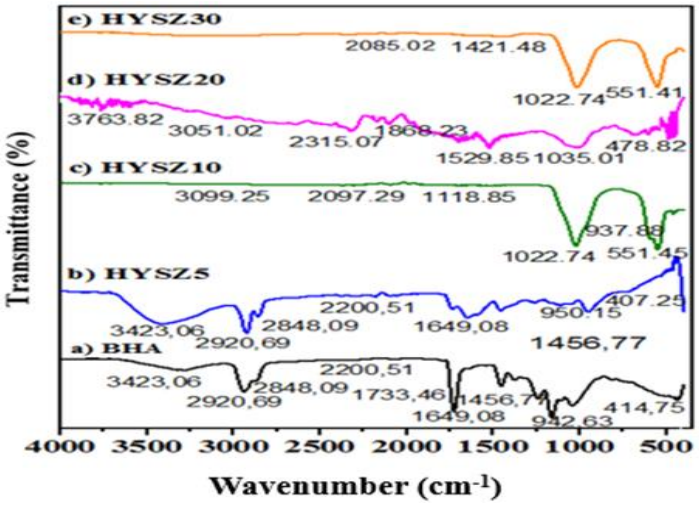

Figure 12. Fourier transform infrared (FTIR) spectroscopy of sintered HA-based composites at 1150°C/ 3h. (a) : HA, (b) : BHA+ 5 % YSZ, (c) : BHA+ 10 % YSZ, (d) : BHA+ 20 % YSZ, (e) : BHA+ 30 % YSZ.

Figure 12 illustrates the results of IR spectroscopy analysis of CaP-ZrO_2 composites sintered at 1150 °C. New groups have appeared in the IR spectra of doped N-HA sintered at 1250 °C. The new bands at 943, 976, 1082, and 1123 cm-1 correspond to the characteristic bands of the PO_4^{3-} groups in the β-TCP phase. A decrease in the intensity of the OH^- band at 3423 cm-1 is observed in the presence of the oxide (ZrO_2) in N-HA. The characteristic bands of the P-O bond in HA, located around 2900 cm^{-1}, have also completely disappeared. This confirms the decomposition of HA into β-TCP. The IR spectroscopy results are in good agreement with the X-ray diffraction results.

3.5. Mechanic characteristic:

The Martans hardness method was used to measure the elastic modulus, applying a 3N load for 15 seconds to verify the influence of the zirconia addition percentage on the Young's modulus evolution.

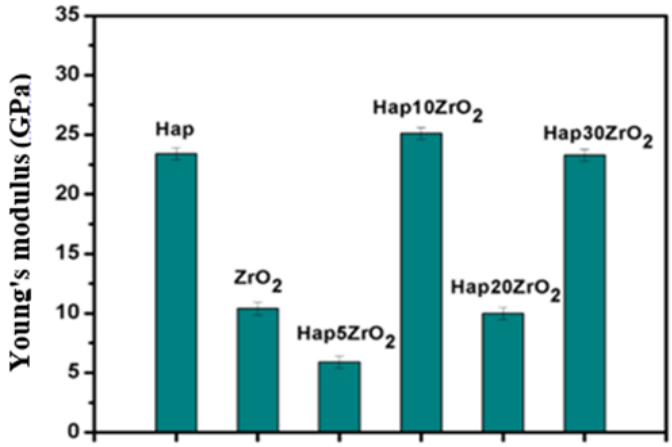

Figure 13. Evolution of Young's modulus as a function of the percentage of zirconia added.

Figure 13 shows the evolution of Young's modulus as a function of the percentage of zirconia added to the samples compacted and sintered at 1150 °C for 2 h. It is very clear that the Young's modulus is not stable and varies from one sample to another. With this type of composite, values ranging from 5.9 GPa to 23.4 GPa were obtained. It is clear that the Young's modulus value is low for the HA+5%ZrO_2 and HA+20%ZrO_2 composites. These values are due to incomplete homogenization and the low sintering temperature, the latter increasing the porosity of the composites. Therefore, the decrease in Young's modulus can be said to be linked to defects such as porosity, which contribute to the degradation of mechanical properties. In other words, the elastic modulus is very sensitive to the shape, size, and distribution of the pores.

Figure 14 shows the displacement/charge-discharge curves of the compacted and sintered samples.

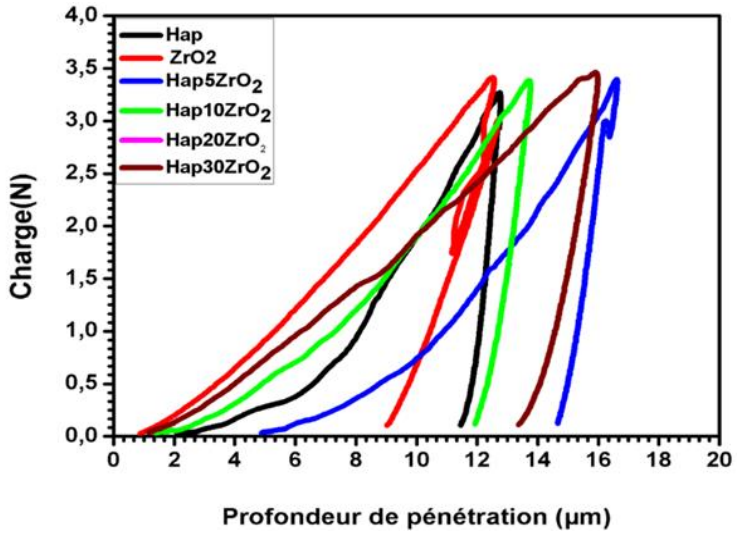

Figure 14. Load-unload/displacement curves obtained by instrumented hardness of compacted and sintered samples.

According to Figure 14, the various compacted and sintered samples underwent elastic and plastic deformation, resulting in residual deformation after unloading. These curves show that the ZrO_2 pellet exhibits better deformation resistance compared to the other pellets: HA (bovine), HA + 5% ZrO_2, HA + 10% ZrO_2, and HA + 30% ZrO_2. These questionable composite results can be attributed to poor homogenization of the mixtures and incomplete sintering of the composites.

Figure 15 represents the variation in Vickers hardness of the composites.

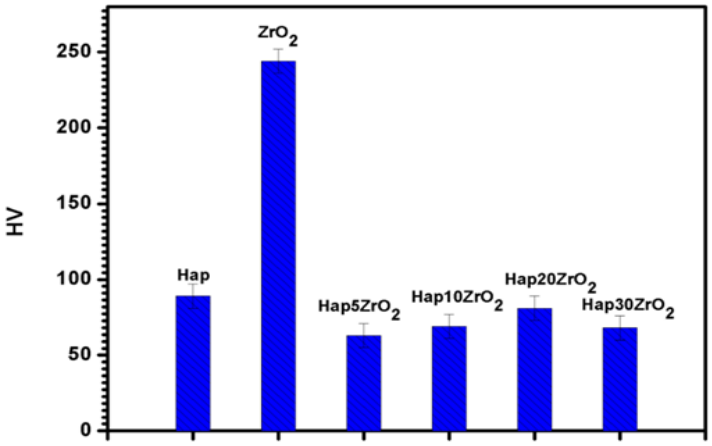

Figure 15. Variation of HV of the composites

According to Figure 15, we can see that the HV value varies from sample to sample; the zirconia pellet shows the highest Vickers hardness with a value of 244 Kp/mm^2, while the minimum value is 63 Kp/mm^2 for the HA+ 5% ZrO_2 composite.

4. **Conclusion**

Calcium phosphate-based composites have great potential due to the advantages derived from the two constituent materials, such as the excellent biocompatibility of HA and the considerable mechanical strength and toughness of ZrO_2.

In this study, we sought to create calcium phosphate-based composites reinforced with varying zirconia content. To this end, we first synthesized the raw material, calcium phosphate, from natural sources. We employed a rigorous methodology, from synthesis to characterization. We obtained the following results:

- Extracting calcium phosphates from biological waste (primarily bone) is an interesting process, not only because of the superior characteristics of the extracted material but also because of the environmental and economic benefits of valorizing this waste.
- Mechanical mixing resulted in a non-uniform distribution of the YSZ phase within the HA matrix.
- The poor mechanical behavior of composites with 0.5 to 30 wt% ZrO_2 is correlated with the presence of porosity and phase distribution heterogeneities, which tend to delay densification.
- Furthermore, the sintering temperature of the HA/ZrO_2 composite caused decomposition of the HA phase.
- Poor densification (porosity) was observed in the composites after sintering in air at 1150°C for 3 hours.

These results confirm the importance of optimizing the sintering temperatures required to achieve better density, while avoiding excessive grain growth.

5. References

[1] Bohner M. Calcium orthophosphates in medicine: From ceramics to calcium phosphate cements. Injury. 2000;31:D37-D47

[2] S. V. Dorozhkin, Bioceramics of calcium orthophosphates, Biomaterials. 31 (2010) 1465–1485. https://doi.org/10.1016/j.biomaterials.2009.11.050.

[3] Wang, J.; Zhu, Y.; Wang, M.; Liu, D.; Chen, X.; Zhu, X.; Yang, X.; Zhang, K.; Fan, Y.; Zhang, X. Fabrication and preliminary biological evaluation of a highly porous biphasic calcium phosphate scaffold with nano-hydroxyapatite surface coating. Ceram. Int. 2018, 44, 1304–1311.

[4] Li, T.T.; Ling, L.; Lin, M.C.; Peng, H.K.; Ren, H.T.; Lou, C.W.; Lin, J.H. Recent advances in multifunctional hydroxyapatite coating by electrochemical deposition. J. Mater. Sci. 2020, 55, 6352–6374.

[5] Asri, R.I.; Harun, W.S.; Hassan, M.A.; Ghani, S.A.; Buyong, Z. A review of hydroxyapatite-based coating techniques: Sol–gel and electrochemical depositions on biocompatible metals. J. Mech. Behav. Biomed. Mater. 2016, 57, 95–108.

[6] Sheykholeslami, S.O.; Fathyunes, L.; Etminanfar, M.; Khalil-Allafi, J. In-vitro biological behavior of calcium phosphate coating applied on nanostructure surface of anodized Nitinol alloy. Mater. Res. Express 2019, 6, 095407

[7] Ranjan, N.; Singh, R.; Ahuja, I. Material processing of PLA-HAp-CS-based thermoplastic composite through fused deposition modeling for biomedical applications. In Biomanufacturing; Springer: Cham, Switzerland, 2019; pp. 123–136.

[8] Fielding, G.A.; Roy, M.; Bandyopadhyay, A.; Bose, S. Antibacterial and biological characteristics of silver containing and strontium doped plasma sprayed hydroxyapatite coatings. Acta Biomater. 2012, 8, 3144–3152.

[9] Thian, E.S.; Huang, J.; Best, S.M.; Barber, Z.H.; Bonfield, W. Magnetron co-sputtered silicon-containing hydroxyapatite thin films—An in vitro study. Biomaterials 2005, 26, 2947–2956.

[10] Linhart W, Briem D, Amling M, Rueger JM, Windolf J. Mechanical failure of porous hydroxyapatite ceramics 7.5 years after implantation in the proximal tibial. Unfallchirurg. 2004;107(2):154-7.

[11] N. Pramanik, D. Mishra, I. Banerjee, T.K. Maiti, P. Bhargava, P. Pramanik Int. J. Biomater., 2009 (2009), p. 512417, 10.1155/2009/512417

[12] SV. Dorozhkin, Calcium orthophosphate-based biocomposites and hybrid biomaterials. J Mater Sci 2009;44(9):2343-87.

[13] Masseli, M.R.; Kuffner, B.H.B.; Vasconcelos, L.V.B.; Silva, G.; Sachs, D. Mechanical and physical characterization of hydroxyapatite/alumina biocomposites produced by the powder metallurgy route for biomedical applications. Mat*é*ria **2021**, 26, 1382.

[14] Orekhov, E.V.; Arbenin, A.Y.; Zemtsova, E.G.; Sokolova, D.N.; Ponomareva, A.N.; Shevtsov, M.A.; Yudintceva, N.M.; Smirnov, V.M.Template Electrochemical Synthesis of Hydroxyapatite on a Titania–Silver Composite Surface for Potential Use in Implantology. Coatings **2022**, 12, 266.

[15] Yuan, X.; Xu, Y.; Lu, T.; He, F.; Zhang, L.; He, Q.; Ye, J. Enhancing the bioactivity of hydroxyapatite bioceramic via encapsulating with silica-based bioactive glass sol. J. Mech. Behav. Biomed. Mater. **2022**, 128, 105104.

[16] Cao, Y.; Shi, T.; Jiao, C.; Liang, H.; Chen, R.; Tian, Z.; Zou, A.; Yang, Y.; Wei, Z.; Wang, C.; et al. Fabrication and properties of zirconia/hydroxyapatite composite scaffold based on digital light processing. Ceram. Int. 2020, 46, 2300–2308.

[17] Rao, R.R.; Kannan, T. Synthesis and sintering of hydroxyapatite-Zirconia composites. Mater. Sci. Eng. C 2002, 20, 187–193.

[18] Wong, J.Y.; Bronzino, J.D.; Wong, J.Y.; Bronzino, J.D. Biomaterials; CRC Press: Boca Raton, FL, USA, 2007.

[19] Chevalier, J. What future for zirconia as a biomaterial, Biomaterials 2006, 27, 535–543.

[20] Cao, Y.; Li, C.; Xia, Y.; Ren, K.; Zhu, S. Study on the fabrication and mechanical properties of HAp-3YSZ composites by flash sintering. Ceram. Int. 2022.

[21] Barakat NA., Khil MS., Omran AM. Sheikh FA. , .Kim HY., Extraction of pure natural hydroxyapatite from the bovine bones biowaste by three different methods. J Mater Process Technol **2009**; 209:3408-3415.

[22] Sharma, S.; Singh, A.; Das, R.M.; Kumar, M. Synthesis of hydroxyapatite Nanoparticles by Modified Co-Precipitation Technique and Investigation of the Ceramic Characteristics upon Thermal Treatment for Their Potential Applications for Water Treatment; CRC Press: Boca Raton, FL, USA, **2022**; 151–169.

[23] Agalya, P.; Kumar, G.S.; Prabu, K.; Cholan, S.; Karunakaran, G.; Hakami, J.; Shkir, M.; Ramalingam, S. One-pot ultrasonic-assisted synthesis of magnetic hydroxyapatite nanoparticles using mussel shell biowaste with the aid of trisodium citrate. Ceram. Int. **2022**; 48: 28299–28307.

[24] A. Raksujarit, K. Pengpat, G. Rujijanagul, T. Tunkasiri, Processing and properties of nanoporous hydroxyapatite ceramics, Materials and Design, **2010**; 31: 1658–1660.

[25] R. B. Heimann and T. A. Vu, Effect of CaO on thermal decomposition during sintering of composite hydroxyapatite-zirconia mixtures for monolithic bioceramic implants, J. Mater. Sci. Lett., **1997**, 16:437–439.

[26] J. M. Wu and T. S. Yeh: J. Mater. Sci., **1988**; 23: 3771.

[27] El-Naggar, M.E.; Abu Ali, O.A.; Saleh, D.I.; Abu-Saied, M.A.; Ahmed, M.K.; AbdelFattah, E.; Mansour, S.F. Microstructure, morphology and physicochemical properties of nanocomposites containing hydroxyapatite/vivianite/graphene oxide for biomedical applications. Luminescence **2021**; 37: 290–301.

[28] H. W. Kim, Y. J. Noh, Y. H. Koh, H. Ee Kim and H. M. Kim: Biomaterials, **2002**; 23: 4113.